Head-on collision of normal rarefaction waves in dusty gases

G. Ben-Dor, O. Igra and T. Elperin
Pearlstone Center for Aeronautical Engineering Studies, Department of Mechanical Engineering, Ben-Gurion University of the Negev, Beer Sheva, Israel

Accepted for publication 30 June 1987

The head-on collision of normal rarefaction waves in dusty gases has been investigated numerically by the modified random choice method with operator splitting techniques. The results were compared with those of a pure gas case.

Keywords: rarefraction waves; dusty gases; two-phase flows

Introduction

The head-on collision of normal rarefaction waves is a classical gas dynamic problem which was first studied in detail by Nicholl[2] more than three decades ago. A schematical illustration of two centered rarefaction waves in the (x, t)-plane and their location at a time before the interaction, $t_1 < t_{CH}$, and after the interaction, $t_2 > t_{CT}$, is shown in Figures 1(a), (b), and (c), respectively. Note that each rarefaction wave consists of a head, H, and tail, T; hence the interaction starts when the two heads collide at $t = t_{CH}$, and it is over when the two tails collide at $t = t_{CT}$.

Prior to the collision (Figure 1(b)), two centered rarefaction waves, R_1 and R_2, propagate one from left to right and the other from right to left into a quiescent gas, state (0). At $t = t_{CH}$ the two heads, H_1 and H_2, collide, and each of them starts penetrating the oncoming opposite rarefaction wave. After the interaction is over, and the two rarefaction waves have penetrated each other, they move apart (Figure 1(c)) as two new rarefaction waves R_3 and R_4. Each of these two rarefaction waves has a head, H_3 and H_4, and a tail, T_3 and T_4. The flow state bounded by these two tails, state (3), is uniform and moves either to the left or to the right, depending on the strengths of the incident rarefaction waves R_1 and R_2.

As mentioned earlier, the head-on collision of normal rarefaction waves was first solved analytically by Steketee[1]. The solution is based on applying the conservation equations[3] separately across each rarefaction wave and imposing the boundary condition of equal pressures and flow velocities behind them.

Owing to the fact that in nature rarefaction waves usually do not propagate in a pure medium, the analytical solution of Steketee[1] is, unfortunately, not sufficient. Alternatively solutions which account for nonhomogeneous flows must be sought. Only such solutions can be used to simulate actual interactions of rarefaction waves.

Unfortunately, however, such solutions cannot be purely analytical, and one is forced to use numerical techniques in order to learn about the interaction of rarefaction waves in dusty gases.

General descriptions and gas-particle suspensions can be found in several review papers and books[4-6]. When the gaseous phase is assumed to be perfect, then the major difference between the case of a pure gas and that of a dusty gas arises from the fact that while the gas responds immediately to the rarefaction wave the dust is much slower to react. As a result, upon the passage of a rarefaction wave the dust-gas suspension which originally was in a state of equilibrium is suddenly changed into a nonequilibrium state. Thereafter heat and momentum exchange start equalizing the gas and dust dynamic and thermodynamic properties until the suspension reaches a new equilibrium state.

Present study

Assumptions

The subsequent analysis is based on the following assumptions, which are usually used when dust-gas suspensions are investigated.

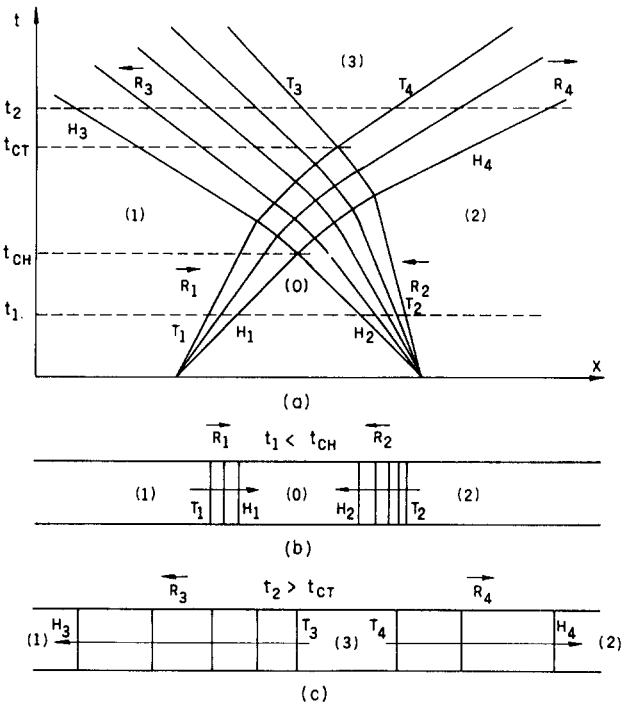

Figure 1 (a) Schematic illustrations of the head-on collision of two rarefaction waves in the (x, t)-plane; (b) schematic illustration of the two incident rarefaction waves, R_1 and R_2, propagating one toward the other before their collision; (c) schematic illustration of the two reflected rarefaction waves, R_3 and R_4, moving away after the interaction was completed

The suspension is assumed to be composed of a thermally perfect inviscid gas and solid particles of spherical shape and uniform size. The volume occupied by the particles is assumed to be negligible since their density is greater by orders of magnitude than that of the gas. The gas and the particles interact with each other through the drag force, D, and the heat transfer rate, Q. The expressions for D and Q, adopted from Miura and Glass[7], are

$$D=\tfrac{1}{8}\pi d^2\rho(u-v)|u-v|C_D \tag{1a}$$

$$Q=\pi d\mu\frac{C_p}{\mathrm{Pr}}(T-\theta)\,\mathrm{Nu} \tag{1b}$$

where

$$C_D=0.48+28\,\mathrm{Re}^{-0.85}$$

$$\mathrm{Nu}=2.0+0.6\,\mathrm{Pr}^{1/3}\mathrm{Re}^{1/2}$$

$$\mathrm{Re}=\frac{\rho|u-v|d}{\mu}$$

$$\mathrm{Pr}=\frac{\mu C_p}{k}$$

In the above expressions u and v are the velocities of the gas and the solid phases, respectively; T and θ are the temperatures of the gas and solid phases, respectively; ρ is the density of the gaseous phase; μ, k, and C_p are the dynamic viscosity, thermal conductivity, and the specific heat capacity at constant pressure of the gaseous phase, respectively; d is the diameter of the solid particles; C_D is the drag coefficient; Re, Nu, and Pr are the Reynolds, Nusselt, and Prandtl numbers, respectively.

Although the validity of the above expressions can be questioned in some cases, the prediction of the suspension properties made on the basis of these expressions were found to be in reasonably good agreement with dusty-shock-tube experimental results[7].

As can be seen from the expressions for the drag force, D, the gravity effects, the Basset force, and the force acting on the solid particle due to pressure gradients are assumed to be negligibly small. The latter assumptions are quite accurate when the solid-gas density ratio is large and pressure gradients are not high.

In addition to the above assumptions, the gas is assumed to be a continuous medium with a molecular mean free path much smaller than the size of the solid particles. As will be shown subsequently, this assumption is valid for the particle size used in the present study. The effect of compressibility, i.e., the dependence of the drag coefficient on the Mach number, can be also neglected for the considered range of flow Mach numbers.

The expression for the heat transfer rate, Q, implies that only convective heat transfer is taken into account. Certainly, when the temperature of the particles becomes high enough, the radiative heat transfer becomes important. In addition to the above assumptions, it was also assumed that the temperature within the solid dust particles is uniform. Finally, it was assumed that the concentration of the solid phase is sufficiently low so that the effect of thermal, mechanical, and/or hydrodynamical interactions between the solid particles can be neglected.

Conservation equations

Under the assumptions presented in the previous section, the one-dimensional nonstationary compressible flow of the gas-dust suspension is governed by the following system of partial differential equations expressing the conservation of mass, momentum, and energy of the gaseous and solid phases:

$$\frac{\partial\rho}{\partial t}+\frac{\partial}{\partial x}(\rho u)=0 \tag{2}$$

$$\frac{\partial}{\partial t}(\rho u)+\frac{\partial}{\partial x}(\rho u^2+P)=-\frac{\sigma}{m}D \tag{3}$$

$$\frac{\partial}{\partial t}[\rho(C_vT+\tfrac{1}{2}u^2)]+\frac{\partial}{\partial x}[\rho u(C_pT+\tfrac{1}{2}u^2)]=-\frac{\sigma}{m}(vD+Q) \tag{4}$$

$$\frac{\partial\sigma}{\partial t}+\frac{\partial}{\partial x}(\sigma v)=0 \tag{5}$$

$$\frac{\partial}{\partial t}(\sigma v)+\frac{\partial}{\partial x}(\sigma v^2)=\frac{\sigma}{m}D \tag{6}$$

$$\frac{\partial}{\partial t}[\rho(C_m\theta+\tfrac{1}{2}v^2)]+\frac{\partial}{\partial x}[\sigma v(C_m\theta+\tfrac{1}{2}v^2)]=\frac{\sigma}{m}(vD+Q) \tag{7}$$

where P is the suspension pressure, σ is the spatial density of the solid phase, m is the mass of a solid particle, C_v is the specific heat capacity at constant volume of the solid phase, and C_m is the heat capacity of the solid particles.

Numerical technique

The above system of partial differential equations was solved numerically by the modified random choice method (RCM) with operator splitting techniques. The RCM represents the combination of the explicit first-order finite difference scheme[8] and the Monte Carlo method. The RCM has been used extensively in gas dynamics[7–9]. However, the RCM employed in this research contains some modifications which considerably improve the quality of the results. The main advantage of the RCM over other numerical schemes is that it allows high resolution of shock waves and contact surfaces, whereas in other finite difference methods they are usually smeared over many grid points as a consequence of artificial viscosity and truncation error of the scheme. The RCM utilizes the exact solution of the Riemann problem with piecewise constant initial data for a finite difference solution of the hyperbolic equations of gas dynamics. The Riemann problem is solved repeatedly between each pair of neighboring spatial grid points. The successive positions of the discontinuities (shock waves, etc.) between these mesh points are sampled with the help of the uniformly distributed sequences of Van der Corput[10]. This implementation of uniformly distributed sequences considerably reduces the numerical noise and thus improves the quality of the results (for more details see Ref. 10).

Some other important details of the random choice scheme applied in the calculations are elaborated in the following. The solution of the Riemann problem with piecewise constant initial data was performed by the iterative method suggested first by Godunov[8]. The homogeneous part of Equations 2–7 was solved by the RCM. The solution is obtained by solving alternatively in each time step the two systems of differential equations. The first system of partial differential equations is derived from Equations 2–7 with the right side set to zero and is solved via the RCM. The second system of equations is derived from Equations 2–7 by omitting the spatial derivatives. The resulting system of ordinary differential equations is then solved with the initial data obtained from the random choice solution. In the calculations the transmissive boundary conditions were assumed for the gaseous and the solid phases.

The initial value problem with piecewise constant initial data for Equations 5–7, describing the flow of the solid particles, was treated analytically[7], assuming the linear distribution of flow variables between adjacent grid points. This approach allows one to preserve the first-order accuracy of the method and

avoids the difficulties arising as a result of the multivalued solution of Equations 5–7.

All the thermodynamic and dynamic variables in Equations 1–7 were nondimensionalized in the following way:

$$\bar{P}=\frac{P}{P^0},\quad \bar{\rho}=\frac{\rho}{\rho_0},\quad \bar{\sigma}=\frac{\sigma}{\sigma_0}$$

$$\bar{u}=\frac{\sqrt{\gamma}u}{a_0},\quad \bar{v}=\frac{\sqrt{\gamma}v}{a_0}$$

$$\bar{T}=\frac{T}{T_0},\quad \bar{\theta}=\frac{\theta}{T_0}$$

$$\tau=\frac{a_0 t}{\sqrt{\gamma}L},\quad \bar{X}=\frac{x}{L}$$

where the subscript 0 refers to the flow state initially separating the two oncoming rarefaction waves, a is the local speed of sound, γ is the specific heat capacities ratio (i.e., $\gamma=C_p/C_v$), and L is a characteristic length. All the calculations were performed with 750 mesh points. The average CPU running time was 4500 s on the CDC Cyber 180-840 computer.

Results and discussions

Pure-gas case

As a first step, the computer code developed for solving the problem at hand was checked by comparing its predictions for the case of a head-on collision of two normal rarefaction waves in a pure gas with those predicted analytically by Steketee[1]. Excellent agreement was obtained.

The two incident rarefaction waves were generated (numerically) by having at $\tau=0$ a high-pressure zone, state (0), separating two lower-pressure zones, states (1′) and (2′), such that $P_{1'}/P_0=0.3$ and $P_{2'}/P_0=0.1$, and $T_0=T_{1'}=T_{2'}$. Thus the strengths of the two incident rarefaction waves were $P_1/P_0=0.53$ and $P_2/P_0=0.28$.

Typical results of the pressure histories are shown in Figures 2(a)–(c). Five pressure histories are shown in Figure 2(a). The two rarefaction waves (R_1 and R_2) are seen to propagate toward each other during $0<\tau<0.196$. At $\tau=0.196$ the heads of R_1 and R_2 collide, and the two rarefaction waves start penetrating each other. The pressure in the area of interaction seems to be practically uniform; however, its value is dropping. At about $\tau=0.256$ the head of R_2 had almost reached the tail of R_1. The head of R_1, however, is still well inside the fan of R_2. Six additional pressure histories are shown in Figure 2(b). The one for $\tau=0.256$, which has already been shown in Figure 2(a), is redrawn for convenience. As can be seen for $\tau>0.256$, the R_3 rarefaction wave starts to form. Its head (marked by an arrowhead) is propagating into state (1). The head of R_1 still propagates inside R_2, until it reaches its tail at about $\tau=0.336$, after which the R_4 rarefaction wave also starts to form. Its head propagates into state (2). At about $\tau=0.532$ the two tails of R_1 and R_2 collide, and the two new rarefaction waves (R_3 and R_4) are fully formed. Thus $\tau=0.532$ corresponds top t_{CT} in Figure 1(a). From this time on R_3 and R_4 move away from each other, leaving between them a constant pressure zone, state (3), as shown in Figure 2(c), where two additional pressure histories are drawn.

Seven temperature histories are shown in Figure 3. At $\tau=0.156$, R_1 and R_2 are seen to propagate toward each other. They collide at about $\tau=0.196$. At about $\tau=0.256$ the head of R_2 reaches the tail of R_1, thus forming the head of R_3. At about $\tau=0.336$ the head of R_1 reaches the tail at R_2, and R_4 is formed. The tails of R_1 and R_2 collide at about $\tau=0.532$. From this time on both R_3 and R_4, which are fully developed, move apart, leaving between them a constant temperature zone, as shown by the temperature history at $\tau=0.632$. Note that, in general, the shape of the temperature histories at any given time is quite similar to that of the pressure at the same instance.

Five histories of the flow velocity are shown in Figure 4.

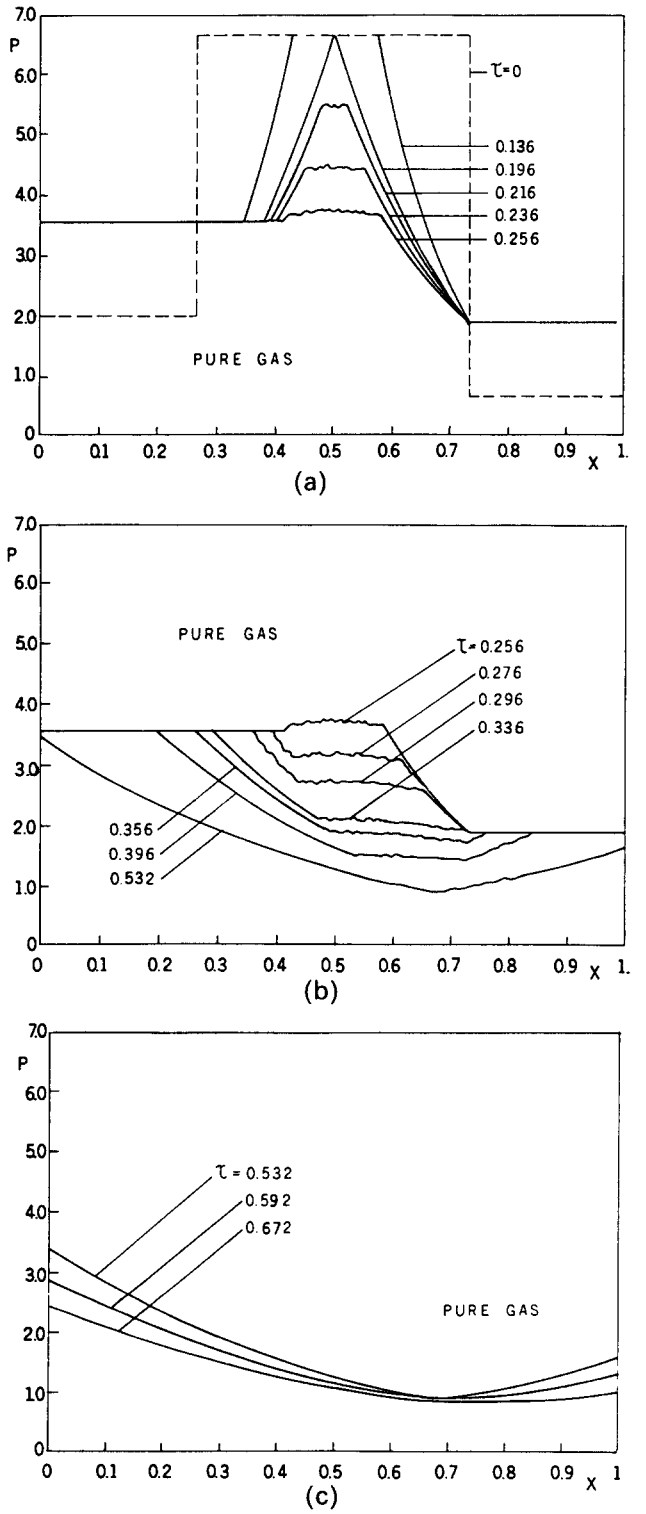

Figure 2 Pressure histories at different instances for the head-on collision of two rarefaction waves in a pure gas

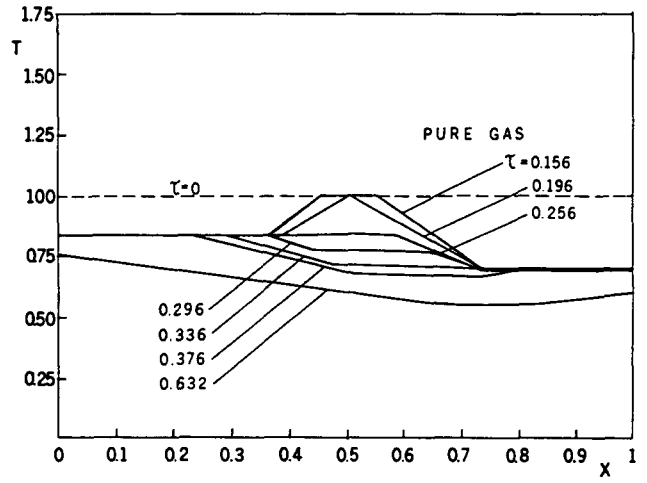

Figure 3 Temperature histories at different instances for the head-on collision of two rarefaction waves in a pure gas

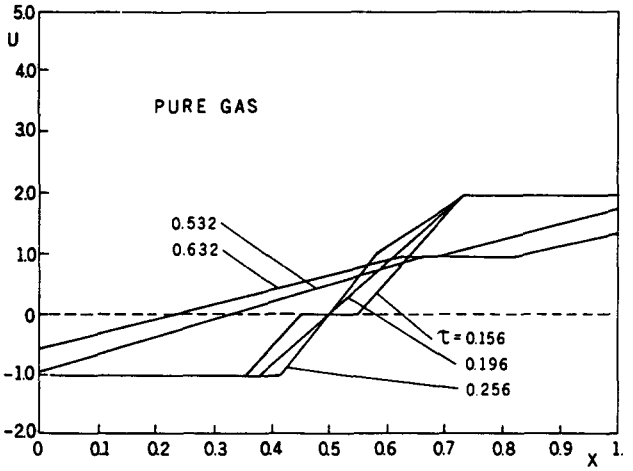

Figure 4 Velocity histories at different instances for the head-on collision of two rarefaction waves in a pure gas

$\tau = 0.156$ corresponds to a time prior to the interactions, $\tau = 0.196$ to a time when the interaction starts, $\tau = 0.532$ to a time when the interaction is completed, and $\tau = 0.632$ to a time after the interaction is over. Figure 4 indicates that the velocity in state (3), between the two transmitted rarefaction waves, is positive. Hence the flow in state (3) follows the R_4 rarefaction wave, i.e., the direction induced by the stronger incident rarefaction wave (R_2 in our case).

Dusty gas case

The results presented in the following are for the same incident rarefaction waves used to illustrate their head-on collision in the case of a pure gas. In addition, state (0) now contains dust. The loading ratio of the dust $\beta = 1$. The dust particle diameter is 10^{-5} cm, and its material density is 2.5 g/cm^3. The two rarefaction waves were initially separated by a distance L and started propagating toward each other at $\tau = 0$.

Fifteen different pressure histories are shown in Figures 5(a)–(c). Comparing Figures 2 and 5 indicates that, in general, the pressure profiles are similar for the dust-free and the dusty gas cases. However, as will be shown subsequently, there is a difference in the absolute value as well as in the propagation velocities. An important feature is that for the pure gas case the interaction was completed at $\tau = 0.532$; but it was completed at only about $\tau = 0.712$ when the gas was seeded with the solid particles. Thus the interaction time is almost 33% longer in the case of a dusty gas.

The eight typical gas temperature histories, T, shown in Figure 6 are quite similar to those obtained for the case of a pure gas (compare with Figure 3). As will be shown subsequently,

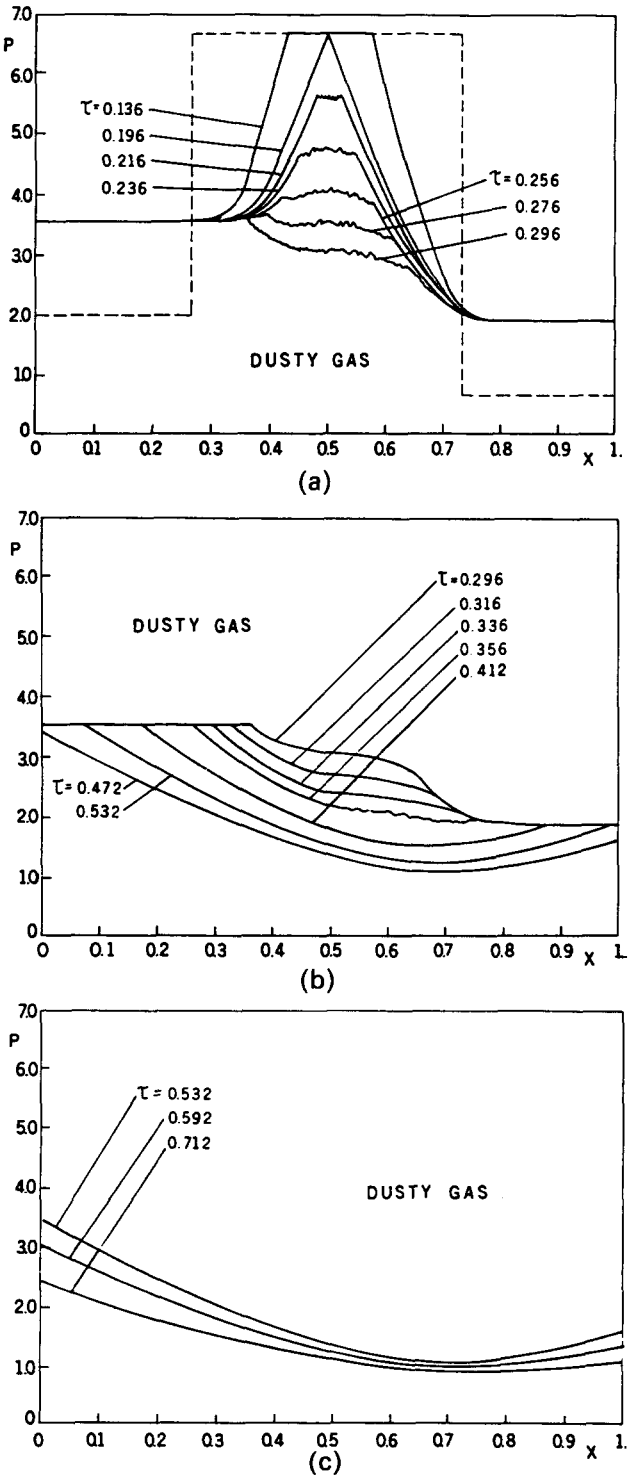

Figure 5 Pressure histories at different instances for the head-on collision of two rarefaction waves in a dusty gas

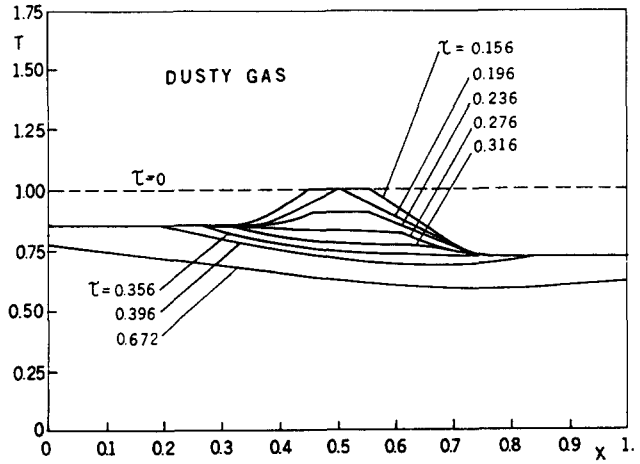

Figure 6 Gas temperature histories at different instances for the head-on collision of two rarefaction waves in a dusty gas

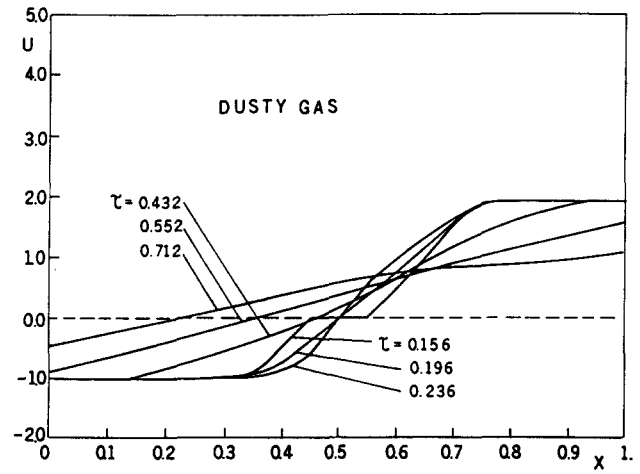

Figure 7 Gas velocity histories at different instances for the head-on collision of two rarefaction waves in a dusty gas

however, the similarity is only in the shape of the profiles but not in the temperature values.

Six typical velocity profiles of the gas velocity, U, are shown in Figure 7. A comparison of Figure 7 with Figure 4 again shows, in general, similar shapes of the profiles. Detailed differences will be discussed separately.

Seven different profiles of the temperature of the solid particles, θ, are shown in Figure 8. Recall that initially the dust particles were present in state (0) only. Thus, the original dust cloud is shown as a dashed line. The two oncoming rarefaction waves R_1 and R_2 sweep the dust particles outwards, as shown for $\tau = 0.176$. At $\tau = 0.216$ the right edge of the dust cloud is already outside the field of view and only the left edge is shown.

The velocity of the solid particles, V, for seven different instances is shown in Figures 9(a) and (b). As can be seen when the interaction is over at $\tau = 0.712$ the particles still have a velocity distribution throughout the entire flow field. Thus a kinematic relaxation between the gaseous and the solid phases, has not been reached yet.

The spatial density, σ, of the solid particles for ten different instances is shown in Figure 10. The dust which initially was concentrated in state (0), shown by the dashed line, is being swept outwards by the two oncoming rarefaction waves. When the interaction is over, $\tau = 0.712$, the dust is almost uniformly distributed throughout the entire flow field.

The temperature profiles of the gas, T, and the solid particles, θ, at four different instances are shown in Figures 11(a)–(c). The solid lines represent the gas temperature, and the dashed lines are for the temperature of the solid particles. Figure 11(a) corresponds to a time prior to the collision. It can be seen that the temperature of the solid particles lags behind the gas temperature. Thus, as expected, the gaseous phase cools down faster than the solid phase. The same behavior is evident at a later time, $\tau = 0.236$, as is shown in Figure 11(b). Figure 11(c) indicates that as time goes on the temperature of the solid particles approaches that of the cooler gas. However, even at $\tau = 0.712$ when the interaction of the two colliding rarefaction waves is over, the solid phase still has a higher temperature than the gaseous phase. Thus, a thermal relaxation between the two phases has not been reached yet.

The velocities of the gas, U, and dust particles, V, are compared in Figures 12(a) and (b). Prior to the collision, Figure 12(a), it is seen that the velocity of the solid particles lags behind that of the gas particles. (Note that on the left side of Figure 12(a) the velocities are negative.) At $\tau = 0.356$ (see Figure 12(b)) the solid-phase velocity is still lagging behind that of the gaseous phase, but the difference between the velocities of the two phases is very small. Similar behavior is seen when the interaction is over at $\tau = 0.712$. The fact that at $\tau = 0.356$ the velocities have almost been equalized while the temperatures (see Figure 11(c)) are still quite different suggests that the momentum exchange mechanism is more efficient than the heat exchange mechanism. Similar results were obtained when we investigated the head-on collision of two normal shock waves in a dusty gas (see Ref. 11 for details). It is also of interest to note that the velocities of the solid particles at $\tau = 0.712$ are greater than those of the gas particles. Thus the solid particles' velocity overshoots the gas velocity before relaxation is finally reached.

Comparison between pure and dusty gases

A comparison between the pressure profiles for the dust-free (dashed lines) and the dusty (solid line) cases is shown in Figures 13(a)–(c) for eight different instances. The pressure profiles prior to the collision at $\tau = 0.176$ are shown in the top of Figure 13(a). The heads of the two incident rarefaction waves (R_1 and R_2) propagate with the local speed of sound, a_0, which is identical for both cases. However, for the pure gas there is a sharp discontinuity in the pressure gradients at the tails of the rarefaction waves (see the kinks, marked by an arrowhead, in the dashed line), but the pressure gradients at the tails of the

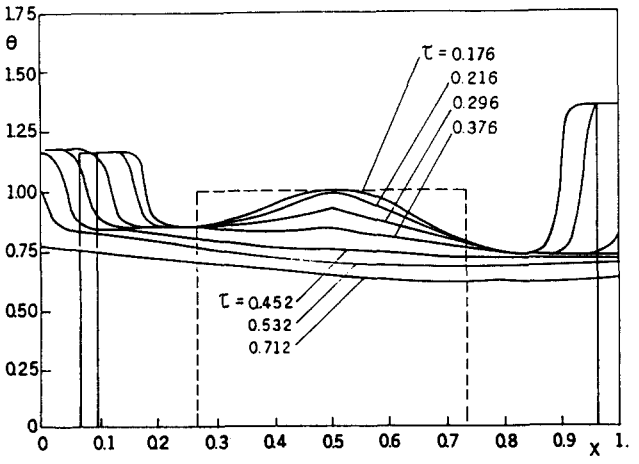

Figure 8 Dust temperature histories at different instances for the head-on collision of two rarefaction waves in a dusty gas

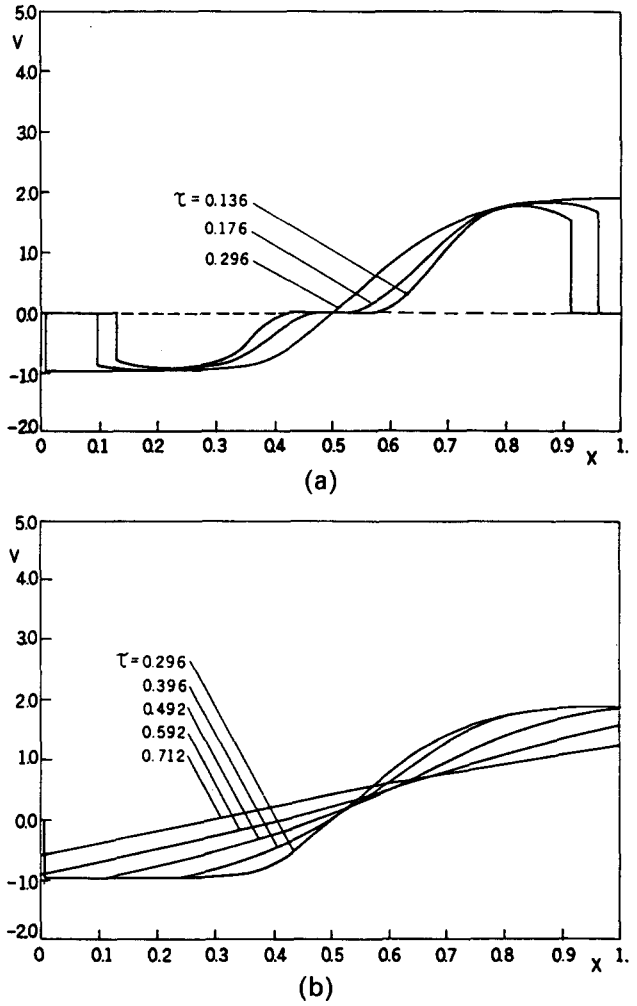

Figure 9 Dust velocity histories at different instances for the head-on collision of two rarefaction waves in a dusty gas

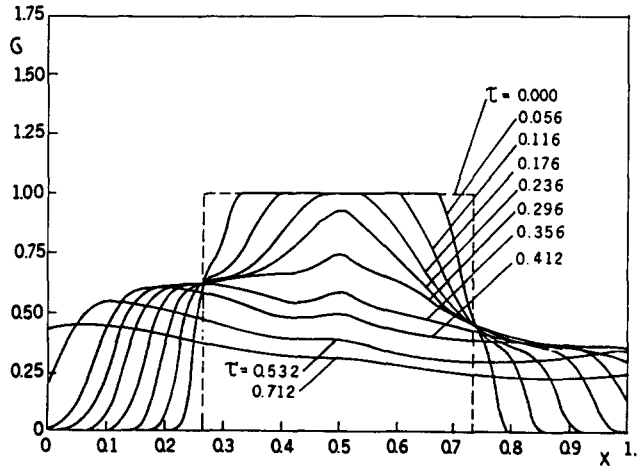

Figure 10 Dust spatial density at different instances for the head-on collision of two rarefaction waves in a dusty gas

rarefaction waves for a dusty gas are continuous and the approach to the back pressure is asymptotic. Furthermore, the tails of the rarefaction waves in the dust-free gas move ahead of the tails for a dusty gas. Thus, the rarefaction waves in dusty gases are wider than they are in pure gases.

The pressure histories at a later time, $\tau = 0.256$, are shown at the bottom of Figure 13(a). In addition to the previously mentioned special features of the structure of the rarefaction waves in dusty gases, it is seen that the pressure is higher inside the interaction zone when the gas is seeded with solid particles. Although for a pure gas the head of R_2 has almost fully penetrated R_1 and almost reached the tail of R_1, for a dusty gas the head of R_2 is still well inside R_1. The top of Figure 13(b) shows the pressure histories at $\tau = 0.336$. At this time, the head of R_2 has emerged from R_1 to form the transmitted rarefaction

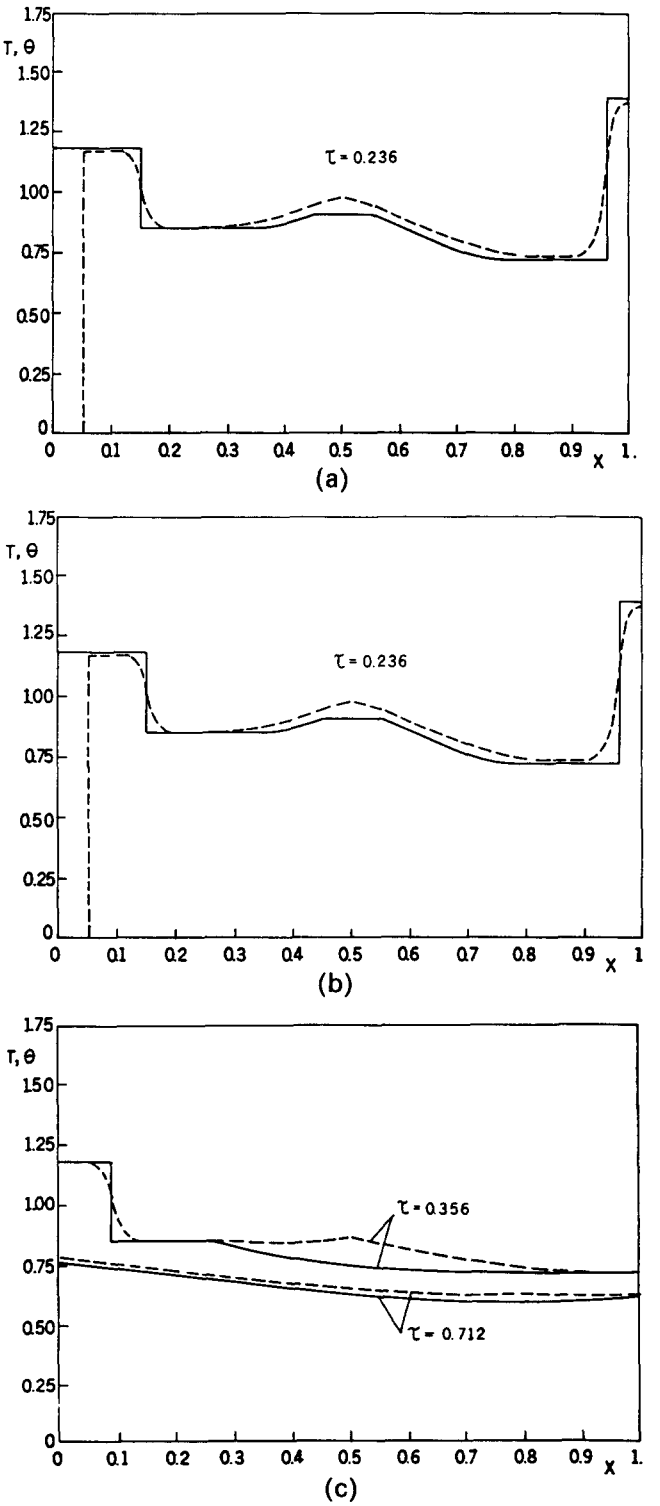

Figure 11 Comparison between the gas and dust temperatures

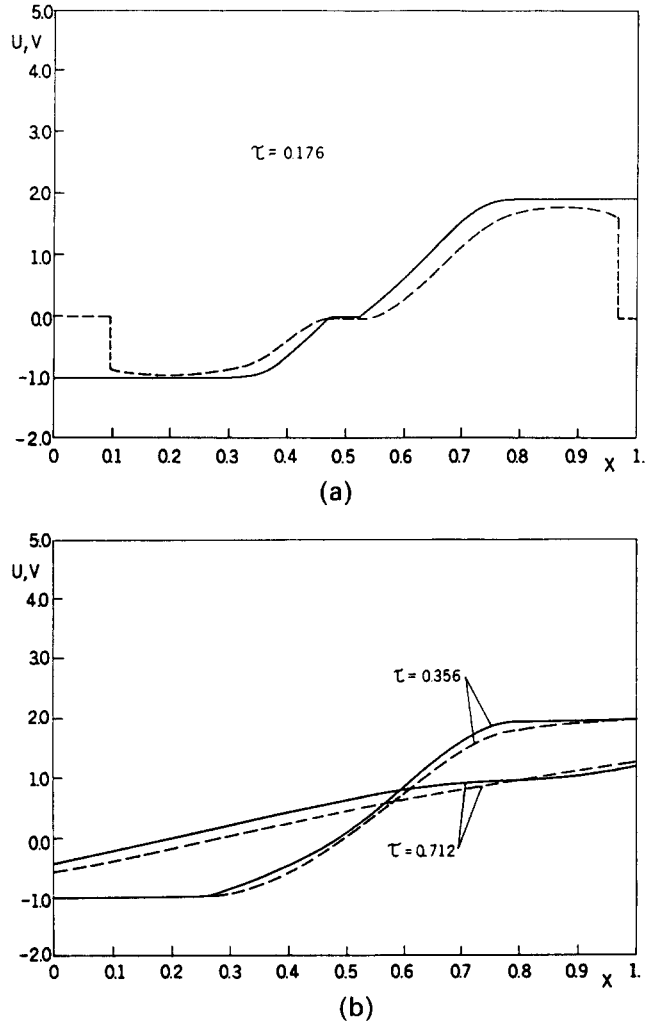

Figure 12 Comparison between the gas and dust velocities

wave R_3, propagating to the left, for both the pure and the dusty cases. Surprisingly, however, the heads of these transmitted rarefaction waves are at the same location. Furthermore, the head of R_1 has almost reached the tail of R_2 in the pure gas while in the dusty gas the head of R_1 (marked by an arrowhead) is still well inside the fan of R_2.

Later ($\tau = 0.376$) when the head of R_1 emerges from R_2 to form the transmitted rarefaction wave R_4, it is again seen that the heads of the transmitted rarefaction waves for both pure and dusty gases are at the same location.

Similar features can be seen at a still later time, $\tau = 0.452$. The pressures are higher for a dusty gas, but the heads of R_3 and R_4 for both cases are practically at the same location. Figure 13(c) describes, in general, the same behavior. However, as time goes on it seems that the pressure differences between the dusty and the pure gas cases decreases. At $\tau = 0.532$, which corresponds to the end of the interaction for the pure gas case, the pressure between the two transmitted rarefaction waves (R_3 and R_4) reached a minimum, which is the new constant pressure in state (3), as shown by the plato in the dashed line at $\tau = 0.632$ and 0.712. Note also that $\tau = 0.712$ corresponds to the end of the interaction in the dusty gas. The minimum pressure finally developed between R_3 and R_4 in the dusty gas is almost identical to the constant pressure obtained in the pure gas.

A comparison between the temperature profiles for pure and dusty gases is shown in Figure 14 for two instances: before the

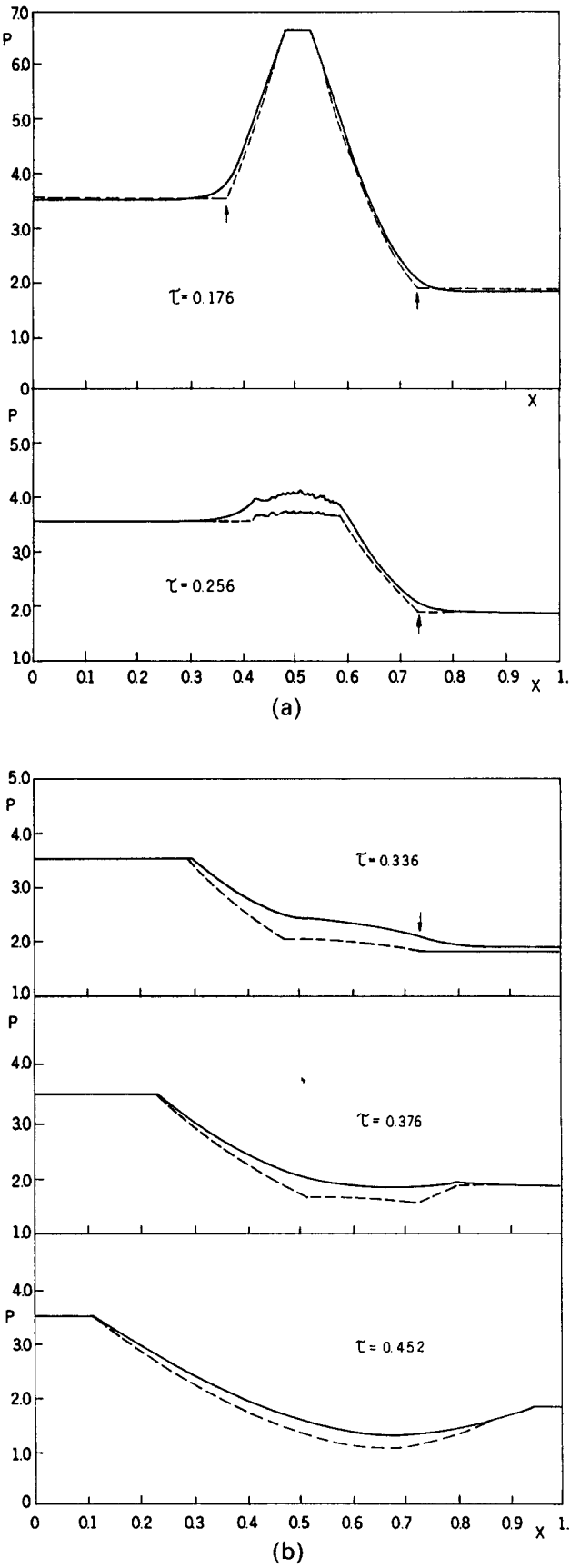

Figure 13 Comparison between the pressures obtained in the head-on collision of rarefaction waves in pure and dusty gases

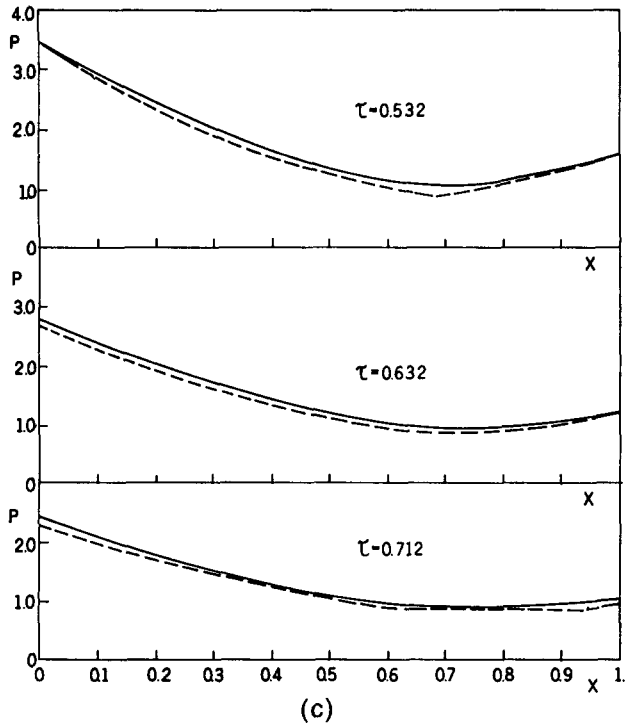

Figure 13 continued

collision, $\tau = 0.176$; and at the end of the interaction in the dusty case, $\tau = 0.712$. It is important to note that the temperatures are higher throughout the flow field for a dusty gas than for a pure gas. However, as time goes on, the differences become smaller and smaller.

The difference in the gas velocities is shown in Figure 15 for three instances. Prior to the collision, at $\tau = 0.176$, it is seen that the gas velocity in the dust-free case is higher than that in the dusty case. This fact is also evident at a later time, $\tau = 0.256$, when the interaction between the two rarefaction waves is taking place. However, an opposite behavior is obtained at a much later time, $\tau = 0.712$, which corresponds to the end of the interaction for the dusty case. At this late time the velocities in the dusty gas case are higher than those in the dust-free case. Also the velocities in the dusty gas approach, toward the end of the interaction, the uniform velocity obtained in state (3) for a dust-free gas.

Summary and conclusions

The head-on interaction of two normal rarefaction waves was solved numerically by the modified RCM with an operator splitting technique. The obtained results were compared to those appropriate to a pure gas.

It was shown that, in general, the profiles of the various gas properties remain similar in their shape to those obtained when the gas is pure, but the values are different. Both the pressures and the temperatures are higher when the gas is seeded with solid particles.

Furthermore, it was shown that the interaction takes longer when the gas is seeded with solid particles.

In addition, special features about the structure of a rarefaction wave in a dusty gas have been pointed out.

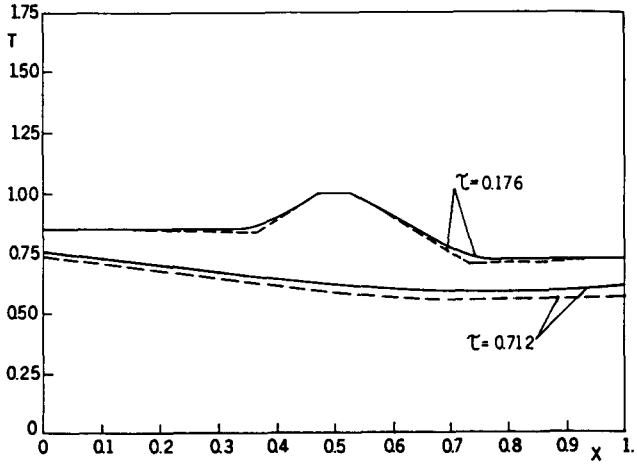

Figure 14 Comparison between the temperatures obtained in the head-on collision of rarefaction waves in pure and dusty gases

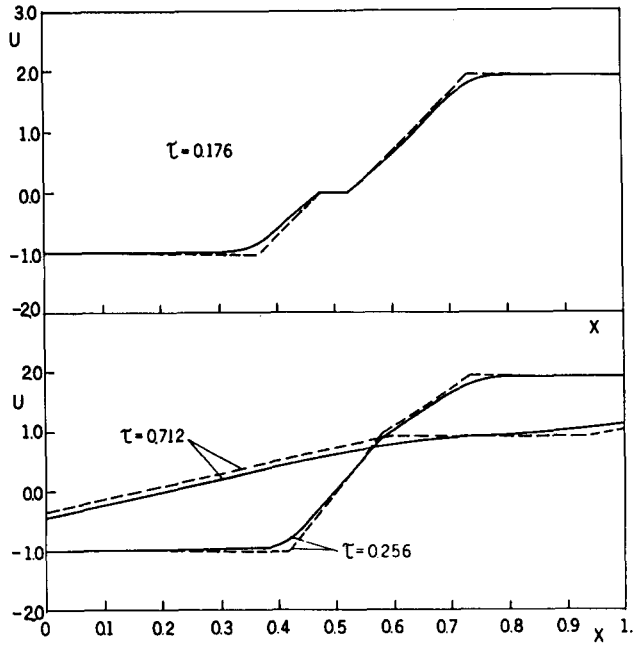

Figure 15 Comparison between the gas velocities obtained in the head-on collision of rarefaction waves in pure and dusty gases

References

1 Steketee, J. A. On the interaction of rarefaction waves in a shock tube. UTIAS, Rev. No. 4, 1952

2 Nicholl, C. I. H. The head-on collision of shock and rarefaction waves. UTIAS Report No. 10, 1951

3 Anderson, J. B. *Modern Compressible Flow*. McGraw-Hill, 1st Ed. 1982

4 Soo, S. L. *Fluid Mechanics of Multiphase Systems*. Blaisdell, Waltham, Mass., 1967

5 Marble, F. E. Dynamics of dusty gases. *Ann. Rev. Fluid Mech.* 1970, **2**, 397–446

6 Rudinger, G. Wave propagation in suspension of solid particles in gas flow. *Appl. Mech. Rev.* 1973, **26**, 273–279

7 Miura, H. and Glass, I. I. On the passage of a shock wave through a dusty layer. *Proc. Roy. Soc. Lond. Ser. A* 1983, **85**, 85–105

8 Godunov, S. K. Finite difference method for numerical calculations of discontinuous solutions of equations of hydrodynamics. *Math. Sbornik*, 1959, **47**, 271–306 (in Russian)

9 Saito, T. and Glass, I. I. Applications of random choice method to problems in gas dynamics. *Prog. Aero. Sci.* 1984, **21**, 201–247

10 Elperin, T. and Igra, O. About the choice of uniformly distributed sequences to be used in the random choice method. *Comp. Methods Appl. Mech. Eng.* 1986, **57**, 181–189

11 Elperin, T., Ben-Dor, G., and Igra, O. Head-on collision of normal shock waves in dusty gases. *Int. J. Heat and Fluid Flow*, 1987, **8**, 303–308